

On using visibility correlations to probe the H I distribution from the dark ages to the present epoch I: Formalism and the expected signal

Somnath Bharadwaj¹ and SK. Sayyad Ali²

Department of Physics and Meteorology
and
Centre for Theoretical Studies
IIT Kharagpur
Pin: 721 302, India

30 October 2019

ABSTRACT

Redshifted 21 cm radiation originating from the cosmological distribution of neutral hydrogen (H I) appears as a background radiation in low frequency radio observations. The angular and frequency domain fluctuations in this radiation carry information about cosmological structure formation. We propose that correlations between visibilities measured at different baselines and frequencies in radio-interferometric observations be used to quantify the statistical properties of these fluctuations. This has an inherent advantage over other statistical estimators in that it deals directly with the visibilities which are the primary quantities measured in radio-interferometric observations. Also, the visibility correlation has a very simple relation with power spectrum. We present estimates of the expected signal for nearly the entire post-recombination era, from the dark ages to the present epoch. The epoch of reionization, where the H I has a patchy distribution, has a distinct signature where the signal is determined by the size of the discrete ionized regions. The signal at other epochs, where the H I follows the dark matter, is determined largely by the power spectrum of dark matter fluctuations. The signal is strongest for baselines where the antenna separations are within a few hundred times the wavelength of observation, and an optimal strategy would preferentially sample these baselines. In the frequency domain, for most baselines the visibilities at two different frequencies are uncorrelated beyond 1 MHz , a signature which in principle would allow the H I signal to be easily distinguished from the continuum sources of contamination.

Key words: cosmology: theory - cosmology: large scale structure of universe - diffuse radiation

1 INTRODUCTION

One of the major problems in modern cosmology is to determine the distribution of matter on large scales in the universe and understand the large scale structure (LSS) formation. The last decade has witnessed phenomenal progress, particularly on the observational front where CMBR anisotropies (eg. Spergel et al. 2003) and galaxy redshift surveys (eg. Tegmark et al. 2003a, 2003b) in conjunction with other observations have determined the parameters of the background cosmological model and the power spectrum of density fluctuations to a high level of precision.

These observations are all found to be consistent with a CDM cosmological model with a scale invariant primordial power spectrum, though there are hints of what could prove to be very interesting features beyond the simplest model.

Another very interesting problem, on smaller scales in cosmology, is the formation of the first gravitationally bound objects and their subsequent merger to produce galaxies. Observations of quasar spectra show the diffuse gas in the universe to be completely ionized at redshifts $z > 5$ (Fan et al. 2002). Understanding the reionization process and its relation with the first generation of luminous objects produced by gravitational collapse is one of the challenges facing modern cosmology.

Observations of the redshifted 21 cm H I radiation pro-

¹ E-mail: somnath@cts.iitkgp.ernet.in

² E-mail: sayyad@cts.iitkgp.ernet.in

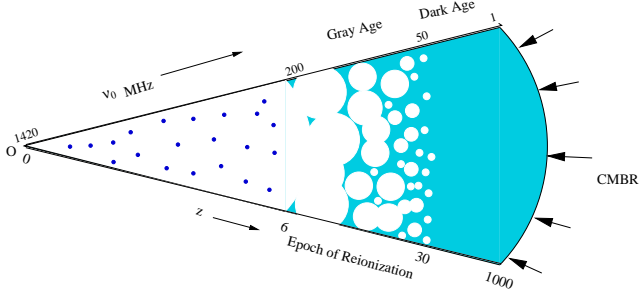


Figure 1. This figure schematically shows the evolution of H I (shaded in the figure) through the entire history of the universe. Hydrogen decouples from the CMBR at $z = 1000$ when electrons and protons combine, for the first time, to produce H I. The subsequent era, until the formation of the first luminous objects at $z = 30$, is referred to as the dark ages or the pre-reionization era. The H I, in the era, is nearly uniformly distributed with small fluctuations which trace the dark matter. The first luminous objects reionize the H I. The reionization is initially confined to small bubbles surrounding the luminous objects. The bubbles of ionized H II gas grow until they finally overlap and the whole universe is reionized by $z = 6$. The H I distribution in the reionization era or the Gray Age is patchy. Only the H I in dense collapsed objects survive the reionization. The surviving H I clouds which are seen as DLAs in quasar absorption spectra are shown as points in the figure. The large scale distribution of these clouds is assumed to follow the dark matter. Also shown is the CMBR which propagates through the intervening H I to the observer at $z = 0$.

vide an unique opportunity for probing the universe from the dark ages when the hydrogen gas first decoupled from the CMBR to the present epoch. Such observations will allow us to probe in detail how the universe was reionized. In addition, redshifted H I observations will allow the large scale distribution of matter in the universe to be studied over a very wide range of redshifts. The possibility of observing 21 cm emission from the cosmological structure formation was first recognized by Sunyaev and Zeldovich (1972). Later studies by Hogan & Rees (1979) and Scott & Rees (1990) consider both emission and absorption against the CMBR.

The cosmological evolution of the H I gas is shown schematically in Figure 1. The 21 cm emission has been perceived as a very important tool for studying the epoch of reionization, and the expected signature, in 21 cm, of the heating of the H I gas and its subsequent reionization has been studied extensively (Madau, Meiksin & Rees 1997; Gnedin & Ostriker 1997; Shaver et al. 1999; Tozzi et al. 2000; Iliev et al. 2002; Iliev et al. 2003; Ciardi & Madau 2003; Furlanetto, Sokasian & Hernquist 2003; Gnedin & Shaver 2003; Miralda-Escude 2003; Chen & Miralda-Escude 2004). The timing, duration and character of the events which led to the reionization of the universe contains an enormous amount of information about the first cosmic structures and also has important implication for the later generations of baryonic objects. This process is not very well understood (eg. Barkana & Loeb 2001), but there are several relevant observational constraints.

The observation of quasars at redshift $z = 6$ which show strong H I absorption (Becker et al. 2001) indicates that at least 1% of the total hydrogen mass at $z = 6$ is neutral (Fan et al. 2002), and the neutral mass fraction decreases rapidly

at lower redshifts. This is a strong indication that the epoch of reionization ended at $z = 6$.

Observations of the CMBR polarization, generated through Thomson scattering of CMBR photons by free electrons along the line of sight, indicates that the reionization began at a redshift $z > 14.0$. On the other hand, the observed anisotropies of the CMBR indicate that the total optical depth of the Thomson scattering is not extremely high, suggesting that reionization could not have started at redshift much higher than about 30 (Spergel et al. 2003).

A third constraint comes from determinations of the IGM temperature from observations of the Ly forest in the z range 2 to 4 which indicates a complex reionization history with there possibly being an order unity change in the neutral hydrogen fraction at $z = 10$ (Theuns et al. 2002; Hui & Haiman 2003).

The possibility of observing the H I emission at $z = 6$, the post-reionization era, has also been discussed extensively particularly in the context of the Giant Metrewave Radio Telescope (GMRT) (Subramanian & Padmanabhan 1993; Kumar, Padmanabhan & Subramanian 1985; Bagla, Nath and Padmanabhan 1997; Bharadwaj, Nath & Sethi 2001; Bagla & White 2002). These observations will probe the large scale structure formation at the redshift where the H I emission originated.

Loeb & Zaldarriaga (2003) have recently proposed that observations of the angular fluctuations in the H I absorptions against the CMBR, originating in the z range 30 to 200 corresponding to the dark age of the universe, would allow the primordial power spectrum to be probed at an unprecedented level of accuracy. Bharadwaj & Ali (2004) have investigated this in detail including the effect of redshift space distortion and gas temperature fluctuations.

In this paper we discuss the nature and the magnitude of the H I signal expected across the entire redshift range starting from the dark age of the universe at $z = 1000$ through the epoch of reionization to the present era. Our discussion is in the context of observations using radio interferometric arrays to study the redshifted H I signal. Such observations are sensitive to only the angular fluctuations in the H I signal. The quantity measured in radio interferometric observations is the complex visibility. Typically, the visibilities are used to construct an image which is then analysed. An image of the H I distribution, while interesting, is not the optimal tool for quantifying and analysing the redshifted H I radiation. The quantities of interest are the statistical properties of the fluctuations in the redshifted H I radiation, and an image, if at all useful, is only an intermediate step in the process of extracting these statistical quantities. Here we propose that correlations between the complex visibilities measured at different baselines and frequencies be used to directly quantify the angular and frequency domain clustering pattern in the H I radiation, completely doing away with the need for making an image.

In Section 2 of this paper we develop the formalism for calculating visibility correlations, bringing out the relation between this quantity and various properties of the H I distribution. The fluctuations, with angle and frequency, of the redshifted H I radiation can be directly related to fluctuations in the properties of the H I distribution in space. The mapping is a little complicated due to the presence of peculiar velocities which moves around spectral features along

the frequency direction. This effect, not included in most earlier calculations, is very similar to the redshift space distortion in galaxy redshift surveys (Kaiser 1987) and has been included here (also Bharadwaj, Nath & Sethi 2001; Bharadwaj & Ali 2004).

The possibility of using visibility correlations to study the H I distribution has been discussed earlier in the restricted context of emission from $z < 6$ by Bharadwaj & Sethi (2001), Bharadwaj & Pandey (2003) and Bharadwaj & Srikant (2004) who have developed the formalism and used it to make detailed predictions and simulations of the signal expected at the GMRT. Also, Morales & Hewitt (2003) have discussed the use of visibility correlations in the context of detecting the H I signal from the epoch of reionization using LOFAR. The work presented here discusses in detail the relation between the visibility correlation and the H I distribution pointing out exactly what such observations would probe. Also, we present rough estimates of the signal expected over the entire history of the H I evolution starting from the dark ages to the present era. Such estimates are expected to be useful in designing optimal observational strategies with existing radio telescopes and also for the design of future radio telescopes optimized for H I observations.

Zaldarriaga, Furlanetto & Hernquist (2003) have proposed the use of the angular power spectrum, in direct analogy with the analysis of the CMBR anisotropies, to quantify the fluctuations in the redshifted H I radiation. It may be noted that this analogy is partially true in that both the redshifted H I radiation and the CMBR are background radiations present at all directions and frequencies. There is a major difference in that observations at different frequencies probe the H I at different distances whereas for the CMBR we expect exactly the same anisotropies at all frequencies. The visibility correlation has an inherent advantage over the angular power spectrum in that it deals directly with visibilities which are the primary quantity measured in radio-interferometric observations. Like the angular power spectrum, the visibility correlation quantifies both the angular fluctuations and the frequency structure of the H I radiation. As we shall see in this paper, the visibility correlation is optimally suited for quantifying radio-interferometric observations of H I radiation, it directly probes the power spectrum and is very simple to interpret.

We next present a brief outline of the paper. In Section 3, we trace the evolution of the cosmological H I from the dark ages to the present era, focusing on epochs which are of interest for 21 cm observations. In Section 4 we present the results for the expected H I signal from the different epochs, and in Section 5 we summarize and discuss our results.

2 THE FORMALISM FOR H I VISIBILITY CORRELATIONS

The story of neutral hydrogen (H I) starts at a redshift $z = 1000$ when, for the first time, the primordial plasma has cooled sufficiently for protons and electrons to combine. The subsequent evolution of the H I is very interesting, we shall come back to this once we have the formulas required to calculate the H I emission and absorption against the CMBR. The propagation of the CMBR, from the last scattering surface where it decouples from the primordial

plasma to the observer at present, through the intervening neutral or partially ionized hydrogen is shown schematically in Figure 1. A long, thin line of sight, the CMBR interacts with the H I through the spin-1/2 hyperfine transition at $\nu = c = \lambda = 1420 \text{ MHz}$ ($\lambda = 21 \text{ cm}$) in the rest frame of the hydrogen. This changes the brightness temperature of the CMBR to

$$T(\nu) = T_{\text{b}} + T_s(1 - e^{-\tau}) \quad (1)$$

where τ is the optical depth, T_{b} is the background CMBR temperature and T_s is the spin temperature defined through the level population ratio

$$\frac{n_1}{n_0} = \frac{g_1}{g_0} \exp(-\tau) \quad (2)$$

Here n_0 and n_1 refer respectively to the number density of hydrogen atoms in the ground and excited states of the hyperfine transition, $g_0 = 1$ and $g_1 = 3$ are the degeneracies of these levels and $T = 0.068 \text{ K} = h_P \nu / k_B$, where h_P is the Planck constant and k_B the Boltzmann constant.

The absorption/emission features introduced by the intervening H I are redshifted to a frequency $\nu = \lambda = (1 + z) \nu_0$ for an observer at present. The expansion of the universe, and the H I peculiar velocity both contribute to the redshift. Incorporating these effects, the optical depth at a redshift z along a line of sight n is (Appendix A)

$$\tau = \frac{4.0 \text{ mK}}{T_s} \frac{b h^2}{0.02} \frac{0.7}{h} \frac{H_0}{H(z)} (1 + z)^3 \frac{H_I}{H} \frac{1}{1} \frac{(1 + z) \partial v}{H(z) \partial r} \quad (3)$$

where r and $H(z)$ are respectively the comoving distance and the Hubble parameter, as functions of z or equivalently n , calculated using the background cosmological model with no peculiar velocities. Also, $H_I = H$ is the ratio of the neutral hydrogen to the mean hydrogen density, and v is the line of sight component of the peculiar velocity of the H I, both quantities being evaluated at a comoving position $x = r n$. The optical depth (eq. 3) is typically much less than unity.

The quantity of interest for redshifted 21 cm observations, the excess brightness temperature redshifted to the observer at present is

$$T_b(n; z) = \frac{T(\nu) - T_{\text{b}}}{1 + z} = \frac{(T_s - T_{\text{b}})}{1 + z} \quad (4)$$

It is convenient to express the excess brightness temperature as $T_b(n; z) = T(z) - H_I(n; z)$ where

$$T(z) = 4.0 \text{ mK} (1 + z)^2 \frac{b h^2}{0.02} \frac{0.7}{h} \frac{H_0}{H(z)} \quad (5)$$

depends only on z and the background cosmological parameters, and

$$H_I(n; z) = \frac{H_I}{H} \frac{1}{1} \frac{T}{T_s} \frac{1}{1} \frac{(1 + z) \partial v}{H(z) \partial r} \quad (6)$$

is the "21 cm radiation efficiency" $(1 - T = T_s) H_I = H$ introduced by Madau, Meiksin & Rees (1997), with the extra velocity term arising here on account of the H I peculiar velocities. We refer to H_I as the "21 cm radiation efficiency in redshift space". This varies with position ($x = r n$) and redshift, and it incorporates the details of the H I evolution

and the effects of the growth of large scale structures. We also introduce $\tilde{\gamma}_{HI}(k; z)$, the Fourier transform of $_{HI}(x; z)$, defined through

$$_{HI}(n; z) = \int_{-Z}^Z \frac{d^3 k}{(2\pi)^3} e^{ik \cdot r \cdot n} \tilde{\gamma}_{HI}(k; z) : \quad (7)$$

and the associated three dimensional power spectrum $P_{HI}(k; z)$ defined through

$$h_{HI}(k; z) \tilde{\gamma}_{HI}(k; z) i = (2\pi)^3 \delta^3(k - k') P_{HI}(k; z) \quad (8)$$

where δ^3 is the three dimensional Dirac delta function.

When discussing radio interferometric observations, it is convenient to use the specific intensity I instead of the brightness temperature. In the Raleigh-Jeans limit $I = 2k_B T = \frac{2}{e} (1+z)^2 T$ where $T = I_{HI}$

$$I = 2.5 \times 10^9 \frac{\text{Jy}}{\text{sr}} \frac{bh^2}{0.02} \frac{0.7}{h} \frac{H_0}{H(z)} \quad (9)$$

The quantities T and I are determined by cosmological parameters whose values are reasonably well established. In the rest of the paper, when required, we shall use equations (5) and (9) with $(m; o; bh^2; h) = (0.3; 0.7; 0.02; 0.7)$ to calculate T and I . The crux of the issue of observing HI is in the evolution $_{HI}$ which is largely unknown. We shall discuss a possible scenario in the next section, before that we discuss the role of $_{HI}$ in radio interferometric observations.

We consider radio interferometric observations using an array of low frequency radio antennas distributed on a plane. The antennas all point in the same direction m which we take to be vertically upwards. The beam pattern $A(\cdot)$ quantifies how the individual antenna, pointing upwards, responds to signals from different directions in the sky. This is assumed to be a Gaussian $A(\cdot) = e^{-\frac{r^2}{\sigma^2}}$ with $\sigma = 1$ i.e. the beam width of the antennas is small, and the part of the sky which contributes to the signal can be well approximated by a plane. In this approximation the unit vector n can be represented by $n = m + \hat{z}$, where \hat{z} is a two dimensional vector in the plane of the sky. Using this I can be expressed as

$$I(n) = I \int_{-Z}^Z \frac{d^3 k}{(2\pi)^3} e^{ik \cdot (k_k + k_z \hat{z})} \tilde{\gamma}_{HI}(k; z) \quad (10)$$

where $k_k = k \cdot m$ and k are respectively the components of k parallel and perpendicular to m . The component k_z lies in the plane of the sky.

The quantity measured in interferometric observations is the complex visibility $V(U; \cdot)$ which is recorded for every independent pair of antennas at every frequency channel in the band of observations. For any pair of antennas, $U = d$ quantifies the separation d in units of the wavelength, we refer to this dimensionless quantity U as a baseline. A typical radio interferometric array simultaneously measures visibilities at a large number of baselines and frequency channels. Ideally, each visibility records a single mode of the Fourier transform of the specific intensity distribution $I(\cdot)$ on the sky. In reality, it is the Fourier transform of $A(\cdot) I(\cdot)$ which is recorded

$$V(U; \cdot) = \int_{-Z}^Z d^2 A(\cdot) I(\cdot) e^{i2\pi U \cdot \hat{z}} : \quad (11)$$

The measured visibilities are Fourier inverted to determine the specific intensity distribution $I(\cdot)$, which is

what we call an image. Usually the visibility at zero spacing $U = 0$ is not used, and an uniform specific intensity distribution makes no contribution to the visibilities. The visibilities record only the angular fluctuations in $I(\cdot)$. If the specific intensity distribution on the sky were decomposed into Fourier modes, ideally the visibility at a baseline U would record the complex amplitude of only a single mode whose period is $1=U$ in angle on the sky and is oriented in the direction parallel to U . In reality, the response to Fourier modes on the sky is smeared a little because of $A(\cdot)$, the antenna beam pattern, which appears in equation (11).

We now calculate the visibilities arising from angular fluctuations in the specific intensity excess (or decrement) $I(\cdot)$ produced by redshifted HI emission (or absorption) against the CMBR. Using eq. (10) in eq. (11) gives us

$$V(U; \cdot) = I \int_{-Z}^Z \frac{d^3 k}{(2\pi)^3} a(U) \frac{r}{2} k_z \tilde{\gamma}_{HI}(k; z) e^{ik \cdot k \cdot r} \quad (12)$$

where $a(U)$ the Fourier transform of the antenna beam pattern $A(\cdot)$

$$A(\cdot) = \int_{-Z}^Z d^2 U e^{i2\pi U \cdot \hat{z}} a(U) : \quad (13)$$

For a Gaussian beam $A(\cdot) = e^{-\frac{r^2}{\sigma^2}}$, the Fourier transform also is a Gaussian $a(U) = \frac{1}{\sigma} \exp\left(-\frac{r^2}{\sigma^2} U^2\right)$ which we use in the rest of this paper.

In equation (12), the contribution to $V(U; \cdot)$ from different modes is peaked around the values of k for which $k_z = 2U = r$. This is so because the visibility $V(U; \cdot)$ responds to angular fluctuations of period $1=U$ on the sky, which corresponds to a spatial period $r=U$ at the distance where the HI is located. It then follows that $\tilde{\gamma}_{HI}(k; z)$ will contribute to a visibility $V(U; \cdot)$ only if the component of k projected on the plane of the sky satisfies $k_z = 2U = r$. The effect of the antenna beam pattern is to introduce a range in k_z of width $j \cdot k_z \approx 2U$ to which each visibility responds.

We use eq. (12) to calculate $hV(U; \cdot)V(U'; \cdot)$, the correlation expected between the visibilities measured at two different baselines U and U' , at two frequencies and $\cdot + \cdot$ which are slightly different i.e. $\cdot = \cdot + \cdot$. The change $\cdot + \cdot$ will cause a very small change in all the terms in eq. (12) except for the phase which we can write as $e^{i2\pi k_z(r + r')}$ where $r' = dr = d$. Using this the visibility correlation is

$$hV(U; \cdot)V(U'; \cdot + \cdot) i = I^2 \int_{-Z}^Z \frac{d^3 k}{(2\pi)^3} a(U) \frac{r}{2} k_z \tilde{\gamma}_{HI}(k; z) a(U') \frac{r'}{2} k_z \tilde{\gamma}_{HI}(k; z) e^{i2\pi k_z(r + r')} \quad (14)$$

The visibilities at U and U' will be correlated only if there is a significant overlap between the terms $a(U) \frac{r}{2} k_z$ and $a(U') \frac{r'}{2} k_z$ which are peaked around different values of k_z . It then follows that visibilities at two different baselines are correlated only if $jU = jU' \approx 1 = (\cdot)$ and the visibilities at widely separated baselines are uncorrelated. To understand the nature of the visibility correlations it will suffice to restrict our analysis to $U = U'$, bearing in mind that the correlation falls off very quickly if $jU = jU' \gg 1 = (\cdot)$. A further simplification is possible if we assume that $U = U' = 2$ for which we can approx-

imate the Gaussian $\langle U \rangle$ with a Dirac delta function using $a^2(jU - (r=2)k_z) \propto (2^3 \delta^2 = r^2) \delta(k_z - (2 = r)U)$ whereby the integrals over k_z in equation (14) can be evaluated. We then have

$$hV(U;)V(U; +)i = \frac{\int_{-2}^2 \int_0^1 dk_k P_{HI}(k) e^{ik_k r}}{4r^2} \quad (15)$$

where $k = k_m + (2 = r)U$. We expect $P_{HI}(k)$ to be an even function of k_z . It then follows that the imaginary part of the visibility correlation is zero, and the real part is

$$hV(U;)V(U; +)i = \frac{\int_{-2}^2 \int_0^1 dk_k P_{HI}(k) \cos(k_z r)}{2r^2} \quad (16)$$

Considering the case $= 0$ first, we see that the visibility correlation $hV(U;)V(U; +)i$ is proportional to $P_{HI}(k)$ integrated over k_z . This directly reflects the fact that a baseline U responds to all Fourier modes k whose projection in the plane of the sky matches $k_z = (2 = r)U$. A mode $k = k_m + (2 = r)U$ satisfies this condition for arbitrary values of k_z which is why we have to sum up the contribution from all values of k_z through the integral. Further interpretation is simplified if we assume that $P_{HI}(k)$ is an isotropic, power law of $k = k_m^2 + (2 = r)^2$ ie. $P_{HI}(k) / k^2$. The integral converges for $n < 1$ for which we have $hV(U;)V(U; +)i / U^{1+n}$ and it is a monotonically decreasing function of U , ie. the correlations will always be highest at the small baselines. This behaviour holds in much of the range of r and U which we are interested in. In general $P_{HI}(k)$ will not be an isotropic function of k , but the qualitative features discussed above will still hold.

The correlation between the visibilities falls as r is increased. To estimate where the visibility correlation falls to zero, we assume that $P_{HI}(k) / k^2$ with $n < 0$. The integral in eq. (16) will have a substantial value if the power spectrum falls significantly before the term $\cos(k_z r)$ can complete one oscillation, and the integral will vanish if the power spectrum does not fall fast enough. Using the fact that the power spectrum will change by order unity when $P_{HI} = P_{HI}$ at $k_z = (2 = r)U = 1$ and that the \cos term completes a full oscillation when $k_z r = 2$, we have an estimate $r = (r)U$ for the value of r beyond which the visibilities become uncorrelated. The point to note is that the fall in the visibility correlation $hV(U;)V(U; +)i$ with increasing r depends on the combination $r = r$ which in turn depends only on z and the cosmological parameters. This holds the possibility of using H I observations to probe the background cosmological model over a large range of z .

In the next section we shall consider a model for the evolution of the H I, and use this to make predictions for the visibility correlations from redshifted 21 cm radiation.

3 THE EVOLUTION OF THE H I

The evolution of the H I is shown schematically in Figure 1. We identify three different eras namely Pre-reionization,

Reionization and Post-reionization and discuss these separately.

3.1 Pre-reionization

We resume the story of H I at the redshift $z = 1000$ where it decouples from the CMBR and the universe enters the Dark Age. Subsequent to this the H I gas temperature T_g is maintained at T by the CMBR which pumps energy into the gas through the scattering of CMBR photons by the small fraction of surviving free electrons. This process becomes ineffective in coupling T_g to T at $z = 200$. In the absence of external heating at $z < 200$ the gas cools adiabatically with $T_g / (1+z)^2$ while $T / (1+z)$. The spin temperature T_s is strongly coupled to T_g through the collisional spin flipping process until $z = 70$. The collisional process is weak at lower redshifts, and T_s again approaches T . This gives a window in redshift $30 < z < 200$ where $T_g < T$ and $T_s < T$. The H I in this redshift range will produce absorption features in the CMBR spectrum. Loeb & Zaldarriaga (2003) have proposed that observations of the angular fluctuations in this signal holds the promise of allowing the primordial power spectrum of density perturbations to be studied at an unprecedented level of accuracy. The nature of this signal was studied in detail in Bharadwaj & Ali (2004), incorporating the effects of peculiar velocities and gas temperature fluctuations.

We assume that all the hydrogen is neutral, and that the fluctuations in the H I density $\delta_{HI}(k; z)$ trace the dark matter fluctuations ie $\delta_{HI}(k; z) = \delta_m(k; z)$. The H I peculiar velocities are also determined by the dark matter, and the Fourier transform of $[1+z] = H(z) @ v = 0$ in equation (6) is $f(m) \cos(k_z r)$, where m is the cosine of the angle between k and the line of sight n , and $f(m) = \frac{1}{m} + \frac{1}{70} \frac{1}{2} m (1 + m)$ in a spatially flat universe Lahav et al. 1991. The fluctuations δ_{HI} also cause fluctuations in the spin temperature T_s which we quantify using a dimensionless function $s(z)$ defined such that $T_s = s T$. Using these in equations (6) and (7) we have the Fourier transform of the 21 cm radiation efficiency in redshift space

$$\tilde{\gamma}_{HI}(k; z) = 1 - \frac{T}{T_s} \frac{i}{1 + f^2} + \frac{T}{T_s} s(k; z) \quad (17)$$

which we use to calculate P_{HI} , the power spectrum of the radiation efficiency in terms of the dark matter power spectrum $P(k)$

$$P_{HI}(k; z) = 1 - \frac{T}{T_s} \frac{i_2}{1 + f^2} + \frac{T}{T_s} s P(k; z) \quad (18)$$

Observations of the angular fluctuations in the H I radiation using either the visibility correlations or other methods like the angular power spectrum will determine P_{HI} (eq. 16). These observations will directly probe the matter power spectrum provided the evolution of $(1 - T / T_s)$ and $s T / T_s$ are known. This has been investigated in detail in Bharadwaj & Ali (2004) and we show the results in Figure 2. The quantities $(1 - T / T_s)$ and $s T / T_s$ also determine the frequencies where we expect a substantial signal.

We use eq. (18) to calculate the visibility correlations expected from the Pre-reionization era.

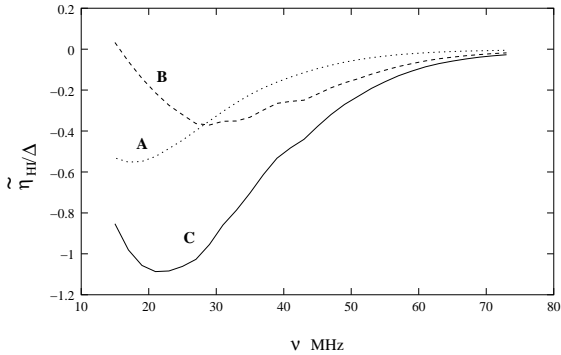


Figure 2. This shows how the 21 cm radiation efficiency in redshift space respond to H I density perturbations, this being quantified by the ratio $\eta_{HI} = (1 - T)/T_s$ (eq. 17). A. shows $(1 - T = T_s)$ which is how it responds through changes in the optical depth, ignoring the effect of peculiar velocities. Peculiar velocities will enhance this effect. B. shows $ST = T_s$ which is how it responds through changes in the spin temperature. C. shows the total response for $S^2 = 2 = 3$.

3.2 Reionization

The Dark Age of the universe ended, possibly at a redshift $z = 30$, when the first luminous objects were formed. The radiation from these luminous objects and from the subsequently formed luminous objects ionized the low density H I in the universe. Initially only small spherical regions (Stromgren sphere) surrounding the luminous objects are filled with ionized H II gas, the rest of the universe being filled with H I (Figure 1). Gradually these spheres of ionized gas grow until they finally overlap, filling up the whole of space, and all the low density gas in the universe is ionized. Here we adopt a simple model for the reionization process. The model, though simple, is sufficiently general to reasonably describe a variety of scenarios by changing the values of the model parameters.

We assume that the H I gas is heated well before it is reionized, and that the spin temperature is coupled to the gas temperature with $T_s = T$ so that $(1 - T = T_s) = 1$. It then follows that $\eta_{HI} > 0$ (eq. 6) i.e. the H I will be seen in emission. Also, the H I emission depends only on the H I density and peculiar velocity. Like in the Pre-reionization era, we assume that the hydrogen density and peculiar velocities follow the dark matter, the only difference being that a fraction of the volume f_V is now ionized. We assume that non-overlapping spheres of comoving radius R are completely ionized, the centres of the spheres being clustered with a bias $b_c = 1$ relative to underlying dark matter distribution. This model is similar to that used by Zaldarriaga, Furlanetto & Hernquist (2003) in the context of H I emission, and Gruzinov & Hu (1998) and Knox et al. (1998) in the context of the effect of patchy reionization on the CMBR. There is a difference in that we have assumed the centres of the spheres to be clustered, whereas Zaldarriaga et al. (2003) assumed them to be randomly distributed. One would expect the centres of the ionized spheres to be clustered, given the fact that we identify them with the locations of the first

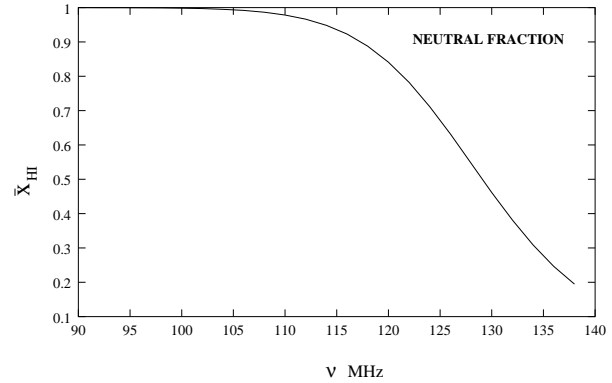


Figure 3. This shows the evolution of the mean neutral fraction x_{HI} with the frequency of the redshifted H I emission for the reionization model discussed in the text.

luminous objects which are believed to have formed at the peaks of the density fluctuations.

The fraction of volume ionized f_V , the mean neutral fraction x_{HI} and mean comoving number density of ionized spheres n_{HI} are related as $f_V = 1 - x_{HI} = (4\pi R^3/3)n_{HI}$. Following Zaldarriaga et al. (2003), we assume that

$$x_{HI}(z) = \frac{1}{1 + \exp((z - z_0)/z)} \quad (19)$$

with $z_0 = 10$ and $z = 0.5$ so that 50% of the hydrogen is reionized at a redshift $z = 10$ (Figure 3). The comoving size of the spheres R increases with z so that it is $3h^{-1} Mpc$ at $z = 10$, and R increases in such a way so that the mean comoving number density of the ionized spheres is constant at $n_{HI} = 4.4 \times 10^3 h^{-3} Mpc^{-3}$.

In this model the H I density is $\eta_{HI}(x; z) = \eta_{HI}(1 + \sum_a (jx - x_a) \delta_R)$ where x is the dark matter fluctuation, a refers to the discrete ionized spheres with centers at x_a , and $\delta_R(y)$ is the Heaviside step function defined such that $\delta_R(y) = 1$ for $0 \leq y \leq 1$ and zero otherwise. We then have

$$\eta_{HI}(x; z) = 1 + \frac{1 + z \delta_R}{H(z) \delta_R} \sum_a \frac{x - x_a}{R} \delta_R \quad (20)$$

We have already discussed the Fourier transform of the first part of eq. (20) which is $(2\pi)^3 \delta_D(k) + (1 + f^2) \delta(k; z)$, and the Fourier transform of the second part is $(2\pi)^3 \delta_D(k) (4\pi R^3/3) W(kR) \sum_a e^{ik \cdot x_a}$ where $W(y) = (3-y^2) \sin(y) y \cos(y)$ is the spherical top hat window function. The term $\sum_a e^{ik \cdot x_a}$ is the Fourier transform of the distribution of the centers of the ionized spheres which we write as $\sum_a e^{ik \cdot x_a} = n_{HI} [(2\pi)^3 \delta_D(k) + \eta_p(k; z) + b_c(k; z)]$, where $\eta_p(k; z)$ is the fluctuation in the distribution of the centers arising due to the discrete nature of these points (Poisson fluctuations) and the term $b_c(k; z)$ arises due to the clustering of the centers. These two components of the fluctuation are independent and $\eta_p(k) \eta_p(k') = (2\pi)^3 \delta_D(k - k') = 1 = n_{HI}$. Convolving the Fourier transform of the two terms in eq. (20), and dropping terms of order f^2 and η_p we have

$$\eta_{HI}(k; z) = x_{HI}(1 + f^2) b_c f_V W(kR) \delta(k; z) \quad (21)$$

This gives the power spectrum of the '21 cm emission efficiency in redshift space" to be

$$P_{\text{HI}}(k; z) = x_{\text{HI}}(1 + f^2) b f_v W(kR)^2 P(k; z) + \frac{f_v^2 W^2(kR)}{n_{\text{HI}}} \quad (22)$$

The first term which contains $P(k)$ arises from the clustering of the hydrogen and the clustering of the centers of the ionized spheres. The second term which has $1 = n_{\text{HI}}$ arises due to the discrete nature of the ionized regions.

Our model has a limitation that it cannot be used when a large fraction of the volume is ionized as the ionized spheres start to overlap. We restrict the model to $z > 10$ where $f_v < 0.5$, and we expect the effect of the overlapping spheres to be small. The possibility of the spheres overlapping also increases if they are highly clustered, and we restrict b_c to $b_c = 1.5$ throughout to keep this under control.

We use equation (22) to calculate the visibility correlations during the Reionization era.

3.3 Post-reionization

All the low density hydrogen is ionized by a redshift $z = 6$ and H I is to be found only in high density clouds (Figure 1), possibly protogalaxies, which survive reionization. Observations of Lyman- α absorption lines seen in quasar spectra have been used to determine the H I density in the redshift range $1 < z < 3.5$. These observations currently indicate $n_{\text{gas}}(z)$, the comoving density of neutral gas expressed as a fraction of the present critical density, to be nearly constant at a value $n_{\text{gas}}(z) = 10^3$ for $z > 1$ (Peroux et al. 2001). The bulk of the neutral gas is in clouds which have H I column densities greater than $2 \times 10^{10} \text{ atom s cm}^{-2}$ (Peroux et al. 2001, Storrie-Lombardi, McMahon & Irwin 1996, Lanzetta, Wolfe & Turnshek 1998). These high column density clouds are responsible for the damped Lyman- α absorption lines observed along lines of sight to quasars. The flux of H I emission from individual clouds (< 10 Jy) is too weak to be detected by existing radio telescopes unless the image of the cloud is significantly magnified by an intervening cluster gravitational lens (Saini, Bharadwaj & Sethi 2001).

We assume that the H I clouds trace the dark matter distribution. Converting n_{gas} to the mean neutral fraction $x_{\text{HI}} = n_{\text{HI}}/H = n_{\text{gas}}/B$ gives us $x_{\text{HI}} = 50 n_{\text{gas}} h^2 (0.02 = B h^2)$ or $x_{\text{HI}} = 2.45 \times 10^{-2}$. We also assume $T_s = T$ and hence we see the H I in emission. Using these we have

$$P_{\text{HI}}(k; z) = x_{\text{HI}}^2 (1 + f^2)^2 P(k; z) \quad (23)$$

The fact that the neutral hydrogen is in discrete clouds makes a contribution which we do not include here. This effect originates from the fact that the H I emission line from individual clouds has a finite width, and the visibility correlation is enhanced when k is smaller than the linewidth of the emission from the individual clouds. Another important effect not included here is that the fluctuations become non-linear at low z . Both these effects have been studied using simulations (Bharadwaj & Srikant 2004). The simple analytic treatment adopted here suffices for the purposes of this paper where the main focus is to estimate the magni-

tude and the nature of the H I signal over a very large range of redshifts starting from the Dark Ages to the present.

4 RESULTS

In this section we present predictions for the visibility correlation signal from the different eras. Equation (16) allows us to calculate the visibility correlation by evaluating just a single integral. This is valid only if $U = (2 \pi)^3$, failing which we have to use eq. (14) which involves a three dimensional integral. Bharadwaj & Pandey (2003) have compared the results calculated using equations (14) and (16), and find that they agree quite well over the range of U of interest. Here we use eq. (16) throughout.

In equation (16), it is necessary to specify σ_0 which is the size of the beam of the individual antennas in the array. It may be noted that $\sigma_0 = 0.6 \text{ FWHM}$. The value of σ_0 will depend on the physical dimensions of the antennas and the wavelength at which the observations are being carried out. We have assumed that $\sigma_0 = 1$ at 325 MHz and scaled this as σ_0/λ to determine the value at other frequencies. This value for σ_0 is appropriate for the GMRT which can operate at frequencies down to 150 MHz. The visibility correlations scale as σ_0^2 , and it is straightforward to scale the results presented here to make visibility correlation predictions for other radio telescopes.

The other input needed to calculate visibility correlations is $P_{\text{HI}}(k)$, the power spectrum of the '21 cm radiation efficiency in redshift space". In the models for the three eras discussed in the previous section, the only quantity which is left to be specified is the dark matter power spectrum $P(k)$ which we take to be that of the currently favoured CDM model with the shape parameter $\sigma_8 = 0.2$, normalized to $\sigma_8 = 1$ at present. We use equations (18), (22) and (23) for $P_{\text{HI}}(k)$ in the pre-reionization, reionization and post-reionization eras respectively.

The visibility correlation $hV(U; \lambda V(U; \lambda))$ responds to the power spectrum at Fourier modes $k = k_{\text{min}} = (2\pi/r)U$. Figure 4 shows the part of the power spectrum which will be probed at different frequencies by the visibility correlations at the baseline $U = 100$. The point to note is that a typical radio interferometric array with a large range of baselines and frequencies will provide many independent measurements of the power spectrum at different epochs and in overlapping bins of Fourier modes. This will allow the evolution of the H I and the dark matter power spectrum to be simultaneously studied at a high level of precision.

4.1 Pre-reionization

The signal here will be absorption features in the CMBR spectrum. The visibility correlations record the angular fluctuations in this decrement. The results for $\sigma_8 = 0$ are shown in Figure 5. The signal is maximum at a frequency 32 MHz where the perturbations in the H I density are most efficient in absorbing the CMBR flux (Figure 2). The signal strength at any fixed frequency does not vary with U in the range of baselines 10 to 100, after which it falls rapidly, falling by an order of magnitude by $U = 1000$. Also, with varying frequency the signal falls off quite fast beyond 45 MHz. Frequencies smaller than 25 MHz will be severely affected

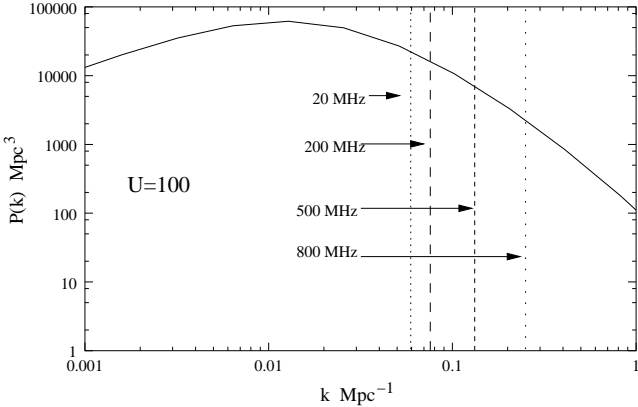


Figure 4. This shows the linear power spectrum of dark matter after density fluctuations used to calculate the expected H I visibility correlations. The power spectrum is shown at the present epoch. A baseline U at a frequency ν will probe the power spectrum at all Fourier modes $k = k_m$ in $(2\pi/r)U$. The values of k_m in are shown at different frequencies for $U = 100$. This figure can be used to determine the length-scale probed by any baselines U .

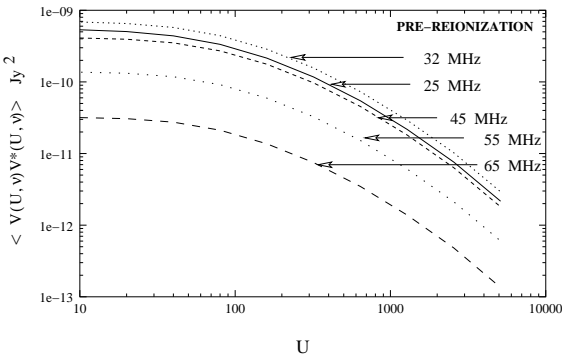


Figure 5. This shows how the visibility correlation $\langle V(U, v)V^*(U, v) \rangle$ varies with baseline U . The results are shown for the different frequencies shown in the figure.

by the ionosphere and have not been shown. The visibility correlations as a function of U have a very similar behaviour at all the frequencies, with just the amplitude of the signal changing with frequency. The shape of these curves directly reflect the power spectrum at the relevant Fourier modes.

The visibility correlation $\langle V(U, v)V^*(U, v) \rangle$ for the same baseline and different frequency is shown for 32 MHz in Figure 6. The behaviour is similar at other frequencies. The correlation falls rapidly as U is increased. The value of U where the visibilities become uncorrelated scales as $U = (r/U)^{1/3}$ and it is around 0.8 MHz for $U = 100$.

4.2 Reionization

The H I signal here is in emission. The results for the visibility correlation $\langle V(U, v)V^*(U, v) \rangle$ are shown as a function of U for different frequencies in Figure 7. At $U = 110$ MHz the hydrogen is largely neutral, and the visibility correlations trace the dark matter power spectrum. The ionization picks

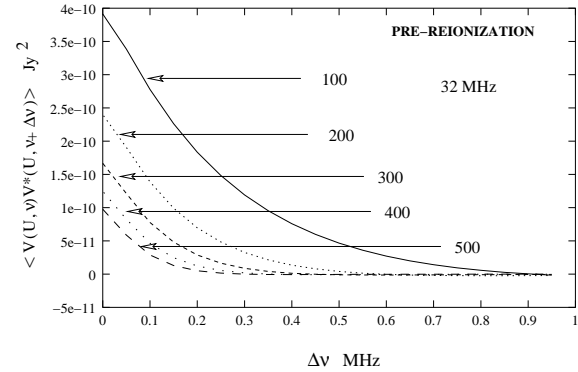


Figure 6. This shows the correlation between the visibilities $V(U, v)V^*(U, v, \Delta v)$ expected for the same baseline U at two slightly different frequencies. The results are shown for different values of U (shown in the figure) for the 32 MHz band.

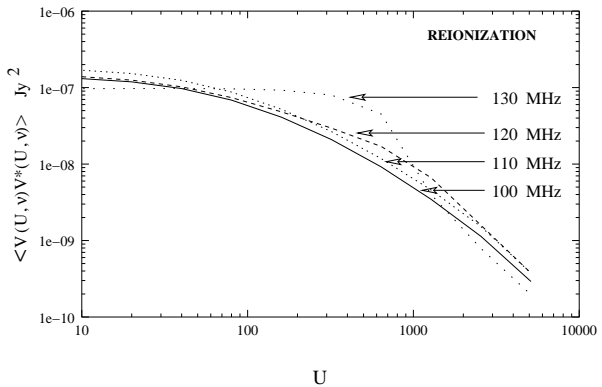


Figure 7. This shows how the visibility correlation $\langle V(U, v)V^*(U, v) \rangle$ varies with baseline U . The results are shown for the different frequencies shown in the figure.

up at $U = 120$ MHz (Figure 3) where ionized bubbles fill up 20% of the universe. The centers of these bubbles are clustered with a bias $b_c = 1.5$ with respect to the underlying dark matter distribution. The presence of these clustered bubbles reduces the signal at small baselines $U < 400$. At 130 MHz around 50% of the universe is occupied by ionized bubbles. Here the clustering of the bubbles or of the underlying dark matter is of no consequence, and the visibility correlations are due to the discrete nature (Poisson distribution) of the ionized bubbles. The visibility correlation falls drastically for the large baselines which resolve out the bubbles, and the signal at $U > 1000$ is due to the clustering of the H I which follows the dark matter. The model for the reionization breaks down when a large fraction of the universe is ionized, and we do not present results beyond 130 MHz.

An interesting feature when the visibility correlation is dominated by the contribution from individual bubbles is that the fall in $\langle V(U, v)V^*(U, v) \rangle$ with increasing U is decided by the ratio $R = r/U$. This follows from the fact

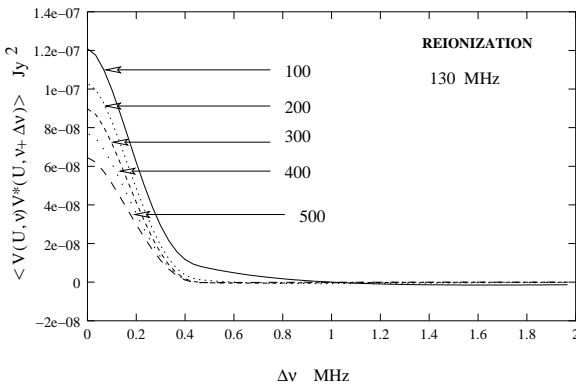


Figure 8. This shows the correlation between the visibilities $V(U; v)$ and $V(U; v + \Delta v)$ expected for the same baseline U at two slightly different frequencies. The results are shown for different values of U (shown in the figure) for the 130 MHz band.

that the power spectrum P_{HI} is now proportional to $W^2(kR)$ which falls rapidly for $k = 1/R$, and the oscillating integral in eq. (16) cancels out when $\theta > R = r$. The value of w where the visibilities become uncorrelated depends only on the size of the bubbles R and does not change with U .

4.3 Post-reionization

The predictions for $\langle V(U; v)V(U; v + \Delta v) \rangle$ are shown as a function of U for a variety of frequencies in Figure 10. At all frequencies the correlations are nearly independent of U in the range 10 to 100, and then fall by nearly an order of magnitude by $U = 1000$. The H I in this era has been assumed to trace the dark matter, and the shape of the curve showing the visibility correlation as a function of U is decided by the dark matter power spectrum at the relevant Fourier modes. The correlations increase with frequency, a reflection of the fact that the matter power spectrum grows with time. At a fixed baseline, the correlation $\langle V(U; v)V(U; v + \Delta v) \rangle$ falls with increasing Δv . The value of w where the visibilities become uncorrelated scales as $w \propto r = r/U$. The predictions for $\Delta v = 500$ MHz are shown in Figure 10 where the visibility at $U = 100$ becomes uncorrelated at $\Delta v \approx 13$ MHz. The behaviour is similar at the other frequencies.

5 SUMMARY AND DISCUSSION.

We have proposed that correlations between the visibilities measured at different baselines and frequencies in radio-interferometric observations be used to quantify and interpret the redshifted 21 cm radiation from cosmological H I. This statistics has an inherent advantage over other quantities which have been proposed for the same purpose in that it deals directly with visibilities which are the primary quantities measured in radio-interferometric observations. There is a further advantage in that the system noise in the visibilities measured at different baselines and frequencies is uncorrelated.

The visibility correlations, we show, have a very simple

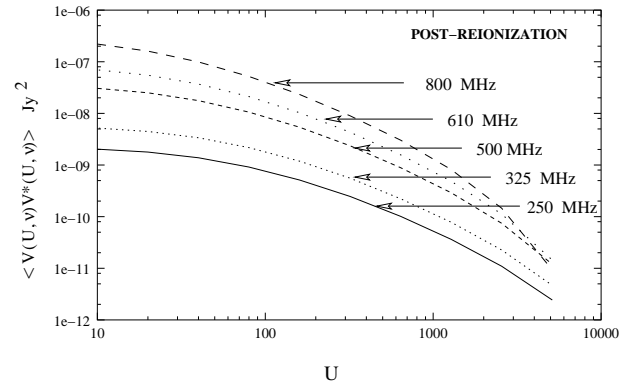


Figure 9. This shows how the visibility correlation $\langle V(U; v)V(U; v + \Delta v) \rangle$ varies with baseline U . The results are shown for the different frequencies shown in the figure.

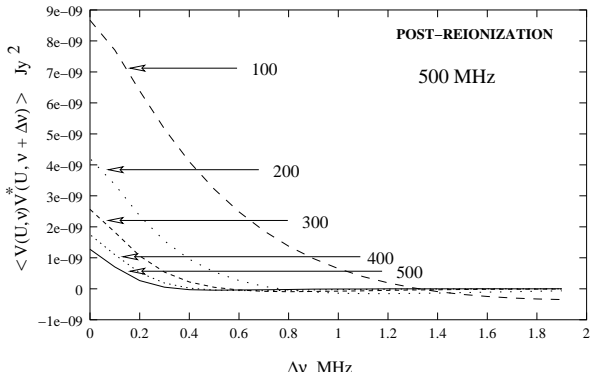


Figure 10. This shows the correlation between the visibilities $V(U; v)$ and $V(U; v + \Delta v)$ expected for the same baseline U at two slightly different frequencies. The results are shown for different values of U (shown in the figure) for the 500 MHz band.

relation to the power spectrum (equation 16), the latter being the statistical quantity most commonly used to quantify the cosmological matter distribution. Also, there is a direct relation between the dimensionless baseline U and the Fourier mode probed by the visibilities at that particular baseline.

We have made predictions for the signal expected over the entire evolution of the H I starting from the dark ages to the present epoch. The magnitude of the signal depends on $\theta = 0.6 \text{ FWHM}$ the size of the beam of the individual antenna elements in the array. Our predictions are for $\theta = 1$ at 325 MHz which is appropriate for the GMRT. At other frequencies we have used θ / θ_0 in making our predictions. The results presented here can be easily used to make predictions for other telescopes using the fact that the visibility correlations scale as θ^2 . The shape of the curves showing $\langle V(U; v)V(U; v + \Delta v) \rangle$ as functions of U or Δv have no dependence on θ or any other parameter of the individual antennas. Finally, a reminder that our analysis

assumes $U = 1$ where the curvature of the sky may be neglected. The analysis will be more complicated for an array of small antennas where the individual elements have a very wide beam, but possibly the qualitative features of this analysis will hold.

One of the salient features of our analysis is that for all the eras the visibility correlation signal from redshifted HI is maximum at small baselines. In the situation where the signal arises mainly from the large scale clustering of the HI whose distribution follows the dark matter the signal is nearly constant up to $U = 100$ after which the signal falls rapidly dropping by an order of magnitude by $U = 1000$. In the situation when the process of reionization is underway and the HI distribution is patchy, the behaviour of the visibility correlation is decided by the size of the ionized regions. In our model for reionization where there are spherical ionized bubbles of comoving radius $R = 3h^{-1} \text{ Mpc}$, the visibility correlation is a constant to $U = 400$, the larger baselines are not sensitive to the ionized spheres. Details of the reionization model aside, the baseline dependence of the visibility correlations is sensitive to size of the ionized patches and it should be possible to extract this information. Also, an optimal observational strategy would preferentially sample the small baselines where the signal is largest. We do not discuss the magnitude of the signal in any detail as this will depend on the telescope parameters.

We next shift our attention to the correlation between the visibilities at the same baseline but at two different frequencies with separation $\Delta\nu$. We see that the correlations fall off very fast as $\Delta\nu$ is increased.

In the situation where the visibility correlation signal is from the large scale gravitational clustering of the HI the value of $\Delta\nu$ where the visibilities become uncorrelated scales as $r = (r/U)$ and it is around 1 MHz at $U = 100$ at all frequencies. In the situation where the signal is from ionized patches, the value of $\Delta\nu$ where the visibilities become uncorrelated is decided by $R = r$ and it is around 0.4 MHz independent of the value of U . This feature should allow us to determine from the observations whether it is the large scale gravitational clustering of the HI or the ionized patches which dominates the visibility correlation. The latter is expected to dominate during the epoch when reionization is underway.

The main challenge in observing cosmological HI is to extract the HI signal from the various contaminants which are expected to swamp this signal. The contaminants include Galactic synchrotron emission, free-free emission from ionizing halos (O'Leary & Mack 2003), faint radio loud quasars (D'Antonio et al. 2002) and synchrotron emission from low redshift galaxy clusters (D'Antonio et al. 2004). Fortunately, all of these foregrounds have smooth continuum spectra whose contribution varies slowly with frequency. The contribution from these contaminants to the visibilities at the same baseline but two frequencies differing by $\Delta\nu$ will remain correlated for large values of U , whereas the contribution from the HI signal will be uncorrelated beyond something like 1 MHz or even less depending on the value of U . It is, in principle, straightforward to fit the visibility correlation at large U and remove any slowly varying component thereby separating the contaminants from the HI signal. We shall investigate in detail issues related to detecting the HI signal, the necessary integration time for different telescopes and signal extraction in a forthcoming paper.

ACKNOWLEDGMENTS

SB would like to thank Jayaram Chengalur for useful discussions. SB would also like to acknowledge BRNS, DAE, Govt. of India, for financial support through sanction No. 2002/37/25/BRNS. SSA is supported by a junior research fellowship of the Council of Scientific and Industrial Research (CSIR), India.

APPENDIX A : THE OPTICAL DEPTH OF THE REDSHIFTED HI 21 CM LINE.

The optical depth is defined as

$$Z_1 = \int_0^1 (1) d\lambda \quad (A1)$$

where (λ) is the absorption coefficient for the redshifted 21 cm line given by

$$= \frac{h_p}{4} e^{- (1) [n_0 B_{01} - n_1 B_{10}]} \quad (A2)$$

Here (λ) is the line profile function, and B_{01} and B_{10} are the Einstein coefficients (Rybicki & Lightman 1979) for the 21 cm line. We use $r(\lambda)$ to denote the comoving distance from which the 1420 MHz radiation will be redshifted to the frequency ν for an observer at present. The HI radiation from a physical line element l at the epoch when the HI radiation originated will be spread over a frequency range

$= (\partial r/\partial \lambda)^{-1} (l-a)$ at the observer. Here $a = 1/(1+z)$ is the scale factor. The line profile function (λ) , defined at the epoch when the HI radiation originated, is a step function of width $a = 1/(1+z)$. It then follows that

$$Z_1 = \int_0^1 \frac{\partial r(\lambda)}{\partial \lambda} d\lambda \quad (A3)$$

and the optical depth can be written as

$$= \frac{h_p}{4} e^{- (1) [g_0 n_0 / g_1 n_1]} a^2 \int_0^1 \frac{\partial r(\lambda)}{\partial \lambda} d\lambda \quad (A4)$$

The Einstein coefficients are related by $B_{01} = 3B_{10} = \frac{3}{2} \frac{e}{h_p c} A_{10}$, where $A_{10} = 2.85 \times 10^{-15} \text{ s}^{-1}$ is the spontaneous emission coefficient of the 21 cm line. So the optical depth finally becomes

$$= \frac{3n_{\text{HI}} h_p c^2 A_{10} a^2}{32 k_B T_{\text{se}}} \int_0^1 \frac{\partial r(\lambda)}{\partial \lambda} d\lambda \quad (A5)$$

where n_{HI} is the number density of HI atoms. In presence of peculiar velocity $r(\lambda)$ is given by

$$r(\lambda) = \frac{cda}{a^2 H(a)} \quad (A6)$$

where v is the line of sight component of the peculiar velocity of the HI. This gives us

$$j \frac{\partial r(\lambda)}{\partial \lambda} = \frac{e}{a^2 H(z)} [1 - \frac{1}{aH(z)} \frac{\partial v}{\partial r}] \quad (A7)$$

where r is the same as $r(\lambda)$ without the effect of peculiar velocities, and where we have retained only the most dominant term in the peculiar velocity. Using this it is possible

to write the optical depth as

$$= \frac{4.0 \text{ m K}}{T_s} \frac{b h^2}{0.02} \frac{0.7}{h} \frac{H_0}{H(z)} (1+z)^3$$

$$\frac{H_I}{H} = 1 - \frac{(1+z)^{3/2}}{H(z)^{1/2}} \quad (A8)$$

where $\frac{H_I}{H}$ is the ratio of the neutral hydrogen to the mean hydrogen density.

REFERENCES

Bagla J.S., Nath B. and Padmanabhan T. 1997, MNRAS 289, 671

Bagla J.S. and White M. 2002, astro-ph/0212228

Barkana R. & Loeb A. 2001, PhysRep., 349, 125

Becker, R. H., et al., 2001, AJ, 122, 2850

Bharadwaj S., Nath B. & Sethi S.K. 2001, JApA 22, 21

Bharadwaj S. & Sethi, S.K. 2001, JApA, 22, 293

Bharadwaj S. & Pandey, S.K. 2003, JApA, 24, 23

Bharadwaj S. & Srikant p.s. 2004, JApA, in press

Bharadwaj S. & Alis S. 2004, MNRAS, in Press,

Chen, X. & Miralda-Escude, J. 2004, ApJ, 602, 1

Ciardi, B. & Madau, P. 2003, ApJ, 596, 1

D' Matteo, T., Ciardi, B., M. Miniati, F. 2004, MNRAS, submitted, astro-ph/0402332

D' Matteo, T., Perna, R., Abel, T., Rees, M. J. 2002, ApJ, 564, 576

Fan, X., et al. 2002, AJ, 123, 1247

Furlanetto, S. R., Sokasian, A. & Hæmquist, L. 2003, astro-ph/0305065

Gnedin, N. Y. & Ostriker, J. P. 1997, ApJ, 486, 581

Gnedin, N. Y. & Shaver, P. A. 2003, astro-ph/0312005

Gruzinov, A. & Hu, W. 1998, ApJ, 508, 435

Hogan, C. J. & Rees, M. J., 1979, MNRAS, 188, 791

Hui, L., & Haiman, Z., 2003, ApJ, 596, 9

Iliev, I.T., Shapiro, P. R., Ferrara, A., Martel, H. 2002, ApJ, 572, L123

Iliev, I.T., Scannapieco, E., Martel, H., Shapiro, P. R. 2003, MNRAS, 341, 81

Kaiser, N. 1987, MNRAS, 227, 1

Kumar, A., Padmanabhan, T. and Subramanian, K., 1995, MNRAS, 272, 544

Knox, L., Scoccimarro, R. & Dodelson, S. 1998, Physical Review Letters, 81, 2004

Lahav, O., Lipje, P. B., Primack, J. R. and Rees, M. J. 1991, MNRAS, 251, 128

Lanzetta, K. M., Wolfe, A. M., Tumshuk, D. A. 1995, ApJ, 430, 435

Loeb, A. & Zaldarriaga, M. 2003, astro-ph/0312134

Madau, P., Meiksin, A. & Rees, M. J., 1997, ApJ, 475, 429

Miralda-Escude, J. 2003, Science 300, 1904-1909

Morales, M. F. and Hewitt, J., 2003, ApJ, submitted (astro-ph/0312437)

Orlo, S. P. & Mack, K. J., 2003, MNRAS, 346, 871

Peroux, C., M. Mahon, R. G., Storrie-Lombardi, L. J. & Irwin, M. J. 2003, MNRAS, 346, 1103

Rybicki, G. B. & Lightman, A. P. 1979, Radiative Processes in Astrophysics, Wiley, New York, pp. 29-32

Saini, T., Bharadwaj, S. & Sethi, K. S. 2001, ApJ, 557, 421

Scott, D. & Rees, M. J., 1990, MNRAS, 247, 510

Shaver, P. A., Winkhorst, R. A., Madau, P. & de Bruyn, A. G. 1999, Astron. & Astrophys., 345, 380

Spergel, D. N., et al. 2003, ApJS, 148, 175

Subramanian, K. and Padmanabhan, T., 1993, MNRAS, 265, 101

Sunyaev, R. A. & Zeldovich, Ya. B., 1972, Astron. & Astrophys., 22, 189

Storrie-Lombardi, L. J., Mahon, R. G., Irwin, M. J. 1996, MNRAS, 283, L79

Tozzi, P., Madau, P., Meiksin, A., Rees, M. J. 2000, ApJ, 528, 597

Tegmark, M., et al., 2003a, ApJ, submitted (astro-ph/0310725)

Tegmark, M., et al., 2003b, ApJ, submitted (astro-ph/0310723)

Theuns, T. et al., 2002, ApJ, 567, L103

Zaldarriaga, M., Furlanetto, S. R. & Hernquist, L., 2003, ApJ, submitted